15th International Plansee Seminar, Eds. G. Kneringer, P. Rödhammer and H. Wildner, Plansee Holding AG, Reutte (2001), Vol. 1

Infiltrated TiC/Cu Composites

N. Frage, N. Froumin, L. Rubinovich and M. P. Dariel

Department of Materials Engineering, Ben-Gurion University of the Negev, P.O.Box 653, Beer-Sheva, Israel

Summary:

One approach for the fabrication of ceramic-metal composites is based on the pressureless impregnation of a porous ceramic preform by a molten metal. Molten Cu does not react with TiC and the wetting angle is close to 90°. Nonetheless, molten Cu readily impregnates partially sintered TiC preforms. A model that describes the dependence of the critical contact angle for spontaneous impregnation by molten metals in partially sintered preforms on the level of densification and on the morphology of the particles was developed. For high aspect ratios of the particles forming the preform, wetting angles close to 90° still allow impregnation by the molten metal. The results of the model were confirmed by infiltration of partially sintered TiC preforms with molten Cu and by fabrication of the TiC/Cu composites with various ceramic-to metal ratios. Decreasing of the metal content in the composite from 50 vol.% to 10 vol.% leads to a hardness increase from 250 to 1800 HV, and to the decrease of the bending strength from 960 to 280MPa. The resistivity of these TiC/Cu composites decreases from 142 ohm·cm to 25 ohm·cm.

Keywords:

Wetting, critical contact angle, infiltration, composite, TiC, Cu

1. Introduction:

Titanium carbide has a high melting point, displays extremely high hardness and shock resistance and its electrical conductivity is comparable to that of

15th International Plansee Seminar, Eds. G. Kneringer, P. Rödhammer and H. Wildner, Plansee Holding AG, Reutte (2001), Vol. 1

metals. Metal-ceramic composites based on the titanium carbide-copper system display a favorable combination of electrical and mechanical properties. Free liquid metal infiltration in a porous ceramic preform is an attractive method for the fabrication of composites over a range of metal-to-ceramic ratios. The main impediment for the fabrication of such composites is the poor wetting of TiC by non-reactive liquid metals such as Cu. The interfacial properties of metal-ceramic systems, and, in particular, the wetting behavior play an important role in the evolution of the microstructure during the processing of metal-ceramic composites. The microstructure is an important factor that determines the mechanical and physical properties of these materials.

Over the past years, the wetting behavior in the TiC/Cu system has been the subject of several investigations (1 - 4). Eremenko in his the early work (1) and later investigators (2 – 4) reported that non-reactive liquid metals like Cu and Ag do not wet stoichiometric TiC and form high 120° contact angles. The addition of titanium to the melt and/or the use of carbon-deficient, hypostoichiometric titanium carbide improve significantly the wetting of the carbide substrate by liquid Cu (2). It has also been established that oxygen is an important and often determining factor of the wetting behavior in metal-ceramic systems (5-7). In titanium carbide, the level of surface oxidation varies from an oxycarbide, TiC_xO_y layer to titanium oxides with different degrees of oxidation (8, 9). Thus, the partial oxygen pressure within the work chamber in the course of some of the processing stages and, in particular, when the carbide is in contact with the liquid metal, is expected to affect the wetting behavior as was previously shown in our work (10). The wetting of ceramics by a molten metal is the outcome of a complex interplay of several factors i.e., the ceramic substrate, the active metal, the molten metal, oxygen and oxide-reducing species. The inter-relationship between these factors is obviously determined by the thermodynamics of this multi-component system.

Pressureless infiltration of a molten metal into the ceramic network is affected by the ability of the liquid metal to wet the ceramic surface. One can easily deduce from elementary physics that the basic requirement for spontaneous, or pressureless infiltration, in a system of cylindrical pores is a negative capillarity pressure, namely a contact angle $\theta<90°$. The driving force for the liquid to penetrate into regular cone-shaped capillaries is proportional to $\cos(\theta-\alpha)$, where α is half of the apex angle of the cone. Thus, even a non-wetting liquid ($\theta > 90°$) may fill a regular cone-shaped capillary. Since the driving force for the liquid impregnation into an inverted cone is proportional to $\cos(\theta+\alpha)$, liquid penetration in such a capillary is possible only for a wetting

15th International Plansee Seminar, Eds. G. Kneringer, P. Rödhammer and H. Wildner, Plansee Holding AG, Reutte (2001), Vol. 1

liquid with $\theta < 90° - \alpha$. An additional requirement for successful liquid metal infiltration is that the porosity of the preforms be interconnected and the liquid and solid do not react to form new phases with a positive excess volume that may plug up the channels. Generally, in real preforms the open channels are tortuous and an interaction may prevail between the ceramic and the metal phases, leading to critical contact angles for spontaneous infiltration that deviate significantly from 90°. This feature was often observed experimentally, for instance, in studies (11-14).

Recently, in an effort to define the relationship between wetting angle and liquid infiltration in a porous structure, Trumble (15,16) has put forward a simple geometrical approach based on the toroid-shaped voids in an assembly of close-packed spheres. According to this model, spontaneous infiltration is limited by liquid penetration into the tetrahedral pores of the close-packed structure for which the critical angle, θ_c=50.7°. A simple geometrical model was also used by Yang and Xi (17) for the spontaneous infiltration into orderly packed fibres or spheres. Even though the authors' approach provides the elements necessary for the analysis of spontaneous infiltration, it still deals with a situation only remotely connected to real systems and the restrictions implicit in the model severely limit its applicability. In particular, the packing mode, the shape of the particles and the surface roughness, as pointed also out by Trumble (15), can differ substantially from those used in the model.

The initial purpose of our study was to examine the possibility of using the infiltration approach for the fabrication of TiC-Cu composites. First experiments indicated, that porous TiC preforms could easily be infiltrated by liquid Cu even though the TiC-Cu system is considered as a non-reactive system. This observation led us to carry out further analysis of pressureless infiltration in sintered or partially sintered powder compacts, by considering the effect of inter-particle neck formation and by relaxing the restriction on the particles shape. In parallel and in an effort to validate the conclusions of the theoretical analysis, we carried out an experimental examination of wetting in the Cu-TiC system. Within this latter part of the study, we determined the properties of the infiltrated TiC/Cu composites over a range of metal-to-ceramic ratios.

2. Experimental Procedure:

Substrates with various levels of porosity were prepared from the titanium carbide powder (ALPHA, Stock #40178, CAS#12070-08-5, typically ~2 μm, purity 99.5%) by uniaxial compaction (100 MPa) and sintering in the 1200-

15th International Plansee Seminar, Eds. G. Kneringer, P. Rödhammer and H. Wildner, Plansee Holding AG, Reutte (2001), Vol. 1

1600°C temperature range for 1 hour, in a vacuum furnace (10^{-4} torr) with a graphite heater. The use of a graphite heater leads to a very low oxygen partial pressure in the work chamber (< 10^{-23} torr) and prevents the oxidation of TiC (18). The porosity of the sintered substrates was measured by the liquid displacement method.
Wetting and impregnation experiments were performed using the sessile drop method at 1150°C in a high vacuum furnace described in more details elsewhere (19). Contact angles were measured directly from the profile images of the molten metal drop. The TiC substrates were polished with 1 μm diamond paste just prior their insertion into the furnace for the contact angle determination. The metal (Cu) used for infiltration was 99,999% pure.
Standard X-ray diffraction, metallographic preparation and EDS methods were used for characterization of the substrates and analysis of the ceramic/metal interfacial regions. The mechanical and electrical properties of the Ti-Cu composites were tested using standard conventional techniques.

3. Results and discussion:

3.1 TiC sample characterization
X-ray diffraction examination revealed the exclusive presence of the TiC phase in the initial powder and the sintered substrates. The level of surface oxidation on the TiC substrates and the oxygen distribution in the near-surface region, as determined by AES analysis combined with Ar depth-sputtering are shown in (Fig.1). The results indicate that sintered titanium carbide had a very low level of oxygen contamination. The oxygen from the surface was completely removed within the first 20-25 sec. of surface sputtering.

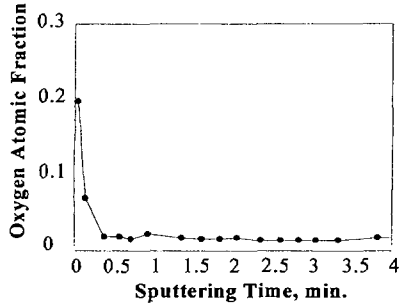

Fig.1. In depth oxygen content in the TiC substrate.

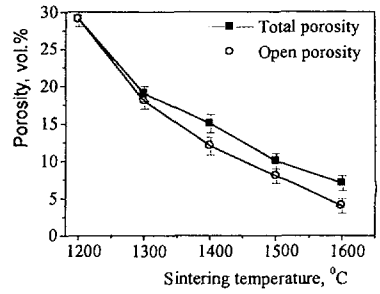

Figure 2. The porosity of the sintered TiC substrates.

15th International Plansee Seminar, Eds. G. Kneringer, P. Rödhammer and H. Wildner, Plansee Holding AG, Reutte (2001), Vol. 1

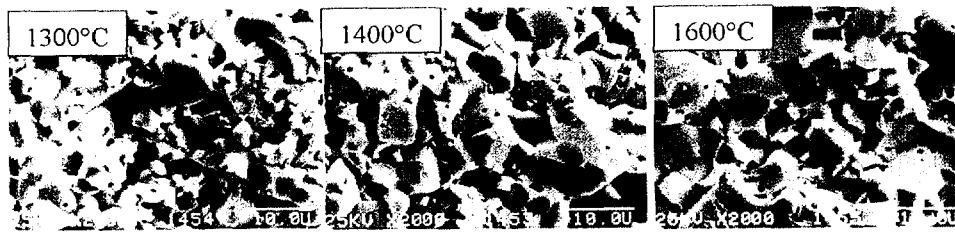

Fig. 3. SEM images of the fracture surfaces of the TiC preforms sintered at three different temperatures.

The porosity of compacted but unsintered substrates was of 45-47 vol.%. The porosity of the samples as a function of the sintering temperature, after a standard 1h treatment, is shown in Fig. 2. The samples reached 94-96 % relative density after pressureless sintering in the range 1500-1600°C and the open porosity was of 5-7%. SEM images of the surface of fractured TiC preforms, sintered at different temperatures, are shown in Fig. 3.
A remarkable grain growth occurs during sintering at elevated temperatures and, as apparent in these figures, the amount of closed porosity increased with increasing sintering temperature.

3.2 Wettability and impregnation of TiC by Cu

Wetting angles were determined on high density TiC substrates. The dependence of the contact angle and of the drop base diameter on the time elapsed after placing the metal on the substrate surface at 1150°C, are shown in Fig. 4. The initial contact angle was about 130° and decreased to a final equilibrium value about 88-89°, after approximately 25 min.

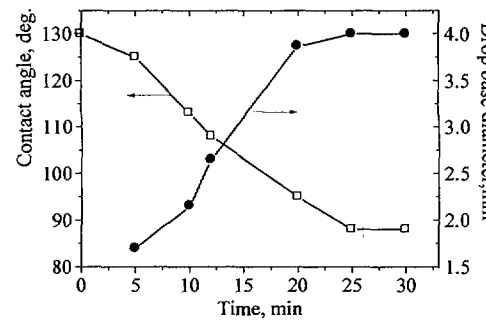

Fig. 4. The contact angles and drop base diameter observed in TiC/Cu systems at 1150°C.

15th International Plansee Seminar, Eds. G. Kneringer, P. Rödhammer and H. Wildner, Plansee Holding AG, Reutte (2001), Vol. 1

Molten Cu impregnates unsintered preforms and also partially sintered substrates, as long as their porosity is higher than 10vol%, without spreading on the surface. Impregnation started after 2-3 min, the incubation period (Fig. 5a), and was completed within ~1 min (Fig. 5 b-e). The outcome of the impregnation was a metal-ceramic composite material.

Fig. 5. The kinetics of Cu impregnation of an unsintered TiC substrate at 1150°C

4. The infiltration of porous preforms. The theoretical model:

4.1 The effect of partial sintering on the critical angle

For a porous structure based on close-packed (FCC, 111) equi-sized spheres (Figs.6a, b), the critical contact angle for spontaneous infiltration, as shown by Tumble (16), can be deduced from simple geometrical considerations. Thus, the liquid penetrates into the non-cylindrical pores until the contact angle with the adjacent solid corresponds to a flat liquid surface.

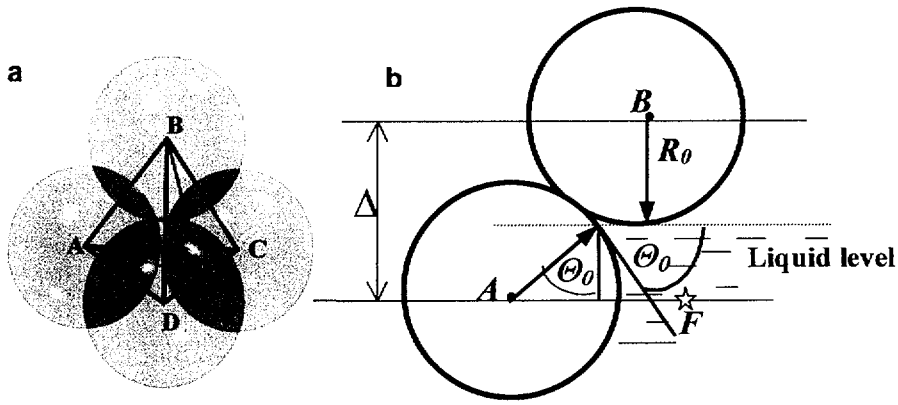

Fig.6. FCC closed-packing of the spherical particles. a) tetrahedral arrangement of the A, B, C and D spheres in FCC structure, b) the section through the centres of A and B spheres and the point F, which is the contact point between D and C spheres, plane ($0\ \bar{1}\ 1$).

15th International Plansee Seminar, Eds. G. Kneringer, P. Rödhammer and H. Wildner, Plansee Holding AG, Reutte (2001), Vol. 1

The conditions for liquid infiltration are fulfilled when the bottom of the next upper layer is tangent to the plane liquid surface. According to the Fig. 6b for the critical contact angle

$$\cos\theta = \frac{\Delta - R_0}{R_0} \tag{1}$$

For the FCC structure (111 layer) with lattice parameter *a*:

$$\Delta = \frac{\sqrt{3}}{3}a, \quad R_0 = \frac{\sqrt{2}}{4}a.$$

According to eq.1 $\cos\theta = \frac{2\sqrt{6}}{3} - 1 = 0.633$ and $\theta = 50.7^0$. The same value for the critical contact angle was obtained by Trumble (16).

In a real assembly of particles, both packing mode and particle shape differ substantially from those used by Trumble. In a partially sintered system the point contact between the particles has grown into a finite boundary area, as shown in Fig. 7.

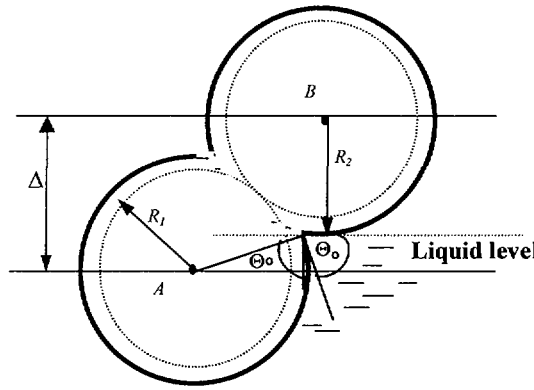

Fig. 7. Packed spheres after partial sintering

During densification stage in the course of the sintering treatment, the centres of the spherical particles approach each other, neck formation occurs and the initial points of contact grow into particle boundaries of finite extension. Since the excess mass at the interface has to be disposed of, one may assume that the radii increase from initial R_0 to R_2, as shown in Fig. 7. As the next step in this model and in order to take advantage of the calculation based on the

15th International Plansee Seminar, Eds. G. Kneringer, P. Rödhammer and H. Wildner, Plansee Holding AG, Reutte (2001), Vol. 1

close-packed arrangement of particles, while we conserve the new inter particle centre distance, we let the spheres contract to new radii R_1, such that the spheres are again only in point contact. We thus obtain a closed packed structure of imaginary spheres that allows us to apply simple geometrical considerations necessary for the evaluation of the relation between porosity and critical contact angle. Notice that this second step in going from R_2 to R_1 is not the reverse of the previous one, namely going from R_0 to R_2. The new system now consists of imaginary spheres in point contact but after some densification had occurred. The critical angle for this case may be found from an equation similar to eq.1, see Fig.7:

$$\cos\theta = \frac{\Delta - R_2}{R_2} \tag{2}$$

It is useful to define a new parameter *g*, which links the R_1 and R_2 radii as $g = 1 - \frac{R_1}{R_2}$ and rewrite eq. (2)

$$\cos\theta = \frac{\Delta}{R_1}(1-g) - 1 \tag{3}$$

Using the relationships for the FCC structure (see above) for the critical contact angle, we obtain

$$\cos\theta = \frac{2\sqrt{6}}{3}(1-g) - 1 \tag{4}$$

For g=0 (unsintered spheres), $\theta = \theta_0 = 50.7°$. However, in general, g>0 and the critical contact angle has a larger value.

We may now derive the relation between the level of sintering (or porosity of the green or partly sintered body) and the critical contact angle. We define a linear contraction parameter $c = 1 - \frac{R_1}{R_0}$ that can be calculated by making use of the law of mass conservation. The mass of original sphere with radius R_0 must be equal to the mass with radius R_2 less 12 spherical segments (cross hatched area in Fig.8), corresponding to the overlap with the 12 neighbours in a close-packed structure (eq. 5)

15th International Plansee Seminar, Eds. G. Kneringer, P. Rödhammer and H. Wildner, Plansee Holding AG, Reutte (2001), Vol. 1

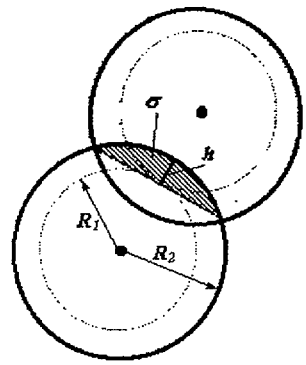

Fig.8. Scheme for calculation of spherical segment (σ) volume. The height of the segment $h=R_1-R_2$

$$\frac{4\pi}{3}R_0^3 = \frac{4\pi}{3}R_2^3 - 12\pi(R_2 - R_1)^2\left(R_2 - \frac{R_2 - R_1}{3}\right) \tag{5}$$

Using the definition of g and from eq.5 we obtain the expression for the contraction parameter:

$$c = 1 - \frac{1-g}{\sqrt[3]{1-3g^2(3-g)}} \tag{6}$$

The porosity of the partially sintered particles with FCC structure (four particles per each cubic cell) can be defined as

$$P = 1 - \frac{(\frac{4\pi}{3}R_0^3)}{(a^3/4)} \tag{7}$$

were $\frac{4\pi}{3}R_0^3$ is the invariant volume of the solid per "Wigner-Seitz" cell of volume $a^3/4$ that decreases gradually in the course of the sintering process. Taking into account the relation between lattice parameter and radius of the imaginary closed-packed spheres ($a = \frac{4R_1}{\sqrt{2}}$) and the definition of the contraction parameter c, the porosity can be expressed as:

$$P = 1 - \frac{\pi\sqrt{2}}{6(1-c)^3} \tag{8}$$

15th International Plansee Seminar, Eds. G. Kneringer, P. Rödhammer and H. Wildner, Plansee Holding AG, Reutte (2001), Vol. 1

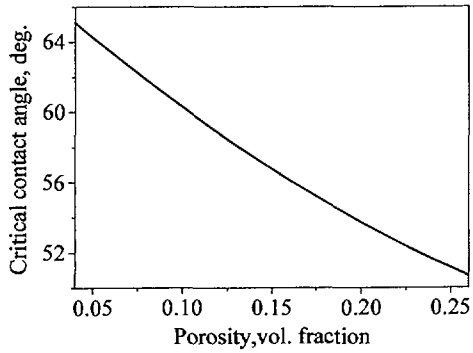

Fig.9. The critical contact angle for partially sintered closed-packed spheres at various levels of porosity.

For a given porosity, eq.(8) allows to calculate *c* and then, using eq.6, the value of *g* and finally the critical contact angle from eq.4. The dependence of the critical contact angle on porosity in the closed packed structure of equi-sized spheres is shown in Fig.9. It, thus, follows that the critical contact angle depends on the level of sintering i.e. on the porosity of the preform.

4.2 The effect of particle shape on the critical angle

A still more realistic description can be attained by relaxing the restriction on the particles shape. First, we consider the extension, by a factor *e*, of the unsintered particles (see Fig.1) in a direction perpendicular to the FCC (111) plane, as shown in Fig.10a.

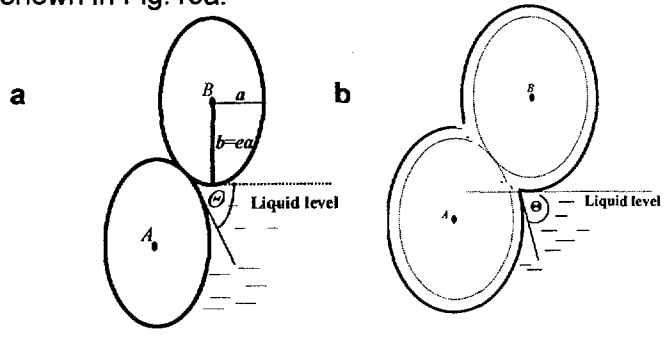

Fig.10. Particles are extended in the direction perpendicular to the packing plane: a) unsintered particles, b) partially sintered particles.

15th International Plansee Seminar, Eds. G. Kneringer, P. Rödhammer and H. Wildner, Plansee Holding AG, Reutte (2001), Vol. 1

The extension transforms the spherical particles into ellipsoids (axes *a* and *b*) with aspect ratio $e=b/a$. The critical contact angle becomes

$$\tan\theta = e \cdot \tan\theta_0 \qquad (9)$$

where θ_0 is the critical contact angle for the closed-packed FCC (111) spheres. The dependence of the critical contact angle on the aspect ratio is shown in Fig.11.

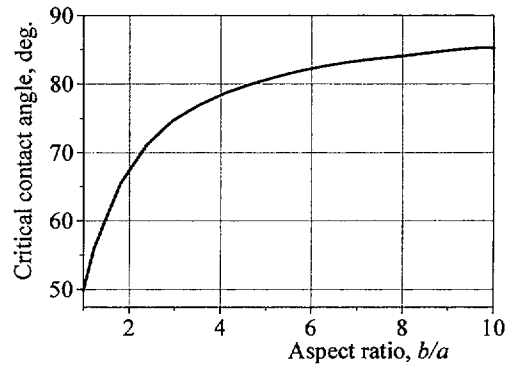

Fig.11. The critical contact angle for various aspect ratios.

For example, for an aspect ratio of particles $e=5$, $\theta = 81°$ and for $e>8$, the critical angle is close to 90°.

4.3 *The critical contact angle, general case*

The simple transformation may be also applied to the partially sintered closed-packed spheres (Fig.10b). We can make use of eq.9 to derive the critical contact angle. The calculated contact angles for partially sintered bodies at different levels of porosity and aspect ratios are shown in Fig.12.

15th International Plansee Seminar, Eds. G. Kneringer, P. Rödhammer and H. Wildner, Plansee Holding AG, Reutte (2001), Vol. 1

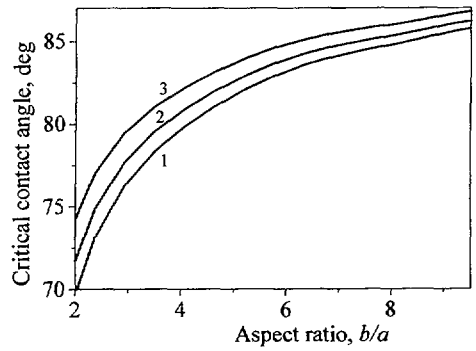

Fig.12. The critical contact angle for partially sintered bodies for various aspect ratios and porosities: 1 - 20%, 2 -15% and 3 –10 vol.%.

Again, as for the unsintered extended spheres, the critical contact angle for more realistic systems is very close to 90°. This situation approaches the cylindrical pore structure for which the classical determination of the critical contact angle (less than 90°) is valid. By relaxing the constraint on the particle shape (ellipsoidal instead of spherical) and allowing some neck formation between adjacent particles, the critical contact angle increased from 50 to about 90°. In a sense these results undermine the critical angle concept, which looses much of its validity. In our discussion, we have brought only a minimum of geometrical modifications to the close-packed equi-sphere model, yet these modifications affect significantly the critical contact angle.
Throughout the analysis, the assumption of non-reacting solid particles with the infiltrating liquid was maintained. The conclusions are hardly applicable to strongly reacting systems, such as molten Cu alloys containing some oxygen and/or titanium in contact with a partly sintered alumina preform. The reaction products at the interface may profoundly alter pore configuration including their closing up. The real non reactive metal-ceramic systems are of interest from still another standpoint. The ceramic particles in these systems conserve their original irregular shape and rough external surface by not undergoing significant dissolution in the liquid. This morphology generates local situations that correspond to particles with a high aspect ratio in contact with the liquid and, as follows from our analysis, increases the critical contact angle.

5. Properties of the infiltrated TiC/Cu composites:

The composites with a various metal-to-ceramic ratio were obtained by infiltration of TiC preforms of different porosity with liquid Cu and the

15th International Plansee Seminar, Eds. G. Kneringer, P. Rödhammer and H. Wildner, Plansee Holding AG, Reutte (2001), Vol. 1

microstructure of these composites are shown in Fig.13. The microstructure of the composites containing more than 30 vol% copper consists of TiC particles embedded in the metal matrix. The irregular shapes of TiC particles may be clearly observed.

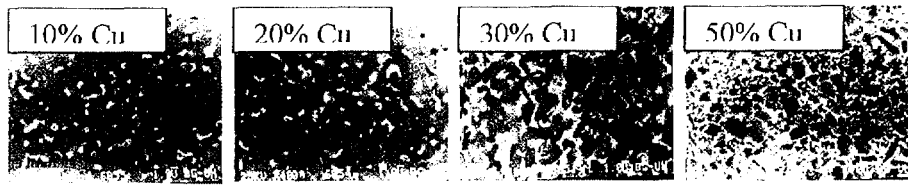

Fig.13. Microstructure of the infiltrated composites with various metal-to-ceramic ratios.

The mechanical and electrical properties of the infiltrated TiC/Cu composites were affected significantly by the ceramic-to-metal ratio. Decreasing of the metal content in the composite from 50 vol.% to 10 vol.% leads to a hardness increase from 250 to 1800HV, and to the decrease of the bending strength from 960 to 280MPa (Fig.14).

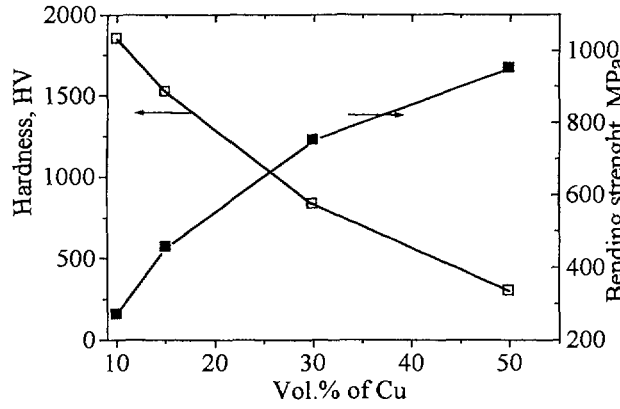

Fig.14. The mechanical properties of the infiltratated TiC/Cu composites.

15th International Plansee Seminar, Eds. G. Kneringer, P. Rödhammer and H. Wildner, Plansee Holding AG, Reutte (2001), Vol. 1

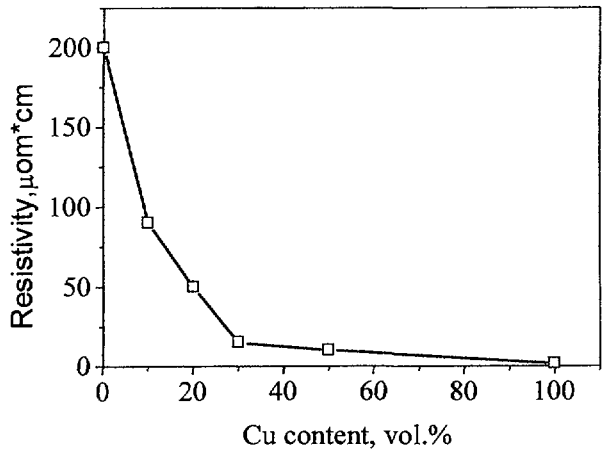

Fig. 15. Electrical resistivity of the infiltrated TiC composites.

The resistivity of these TiC/Cu composites (Fig.15) decreases rapidly from 142 μohm·cm to 25 μohm*cm at 30 vol% Cu, in agreement with the microstructure shown in Fig. 13. At higher Cu contents, the resistivity decreases gradually to values corresponding to pure Cu.

Conclusions:

A model was developed to account for the dependence of the critical contact angle for spontaneous impregnation by molten metals, in partially sintered preforms, on the level of densification and on the morphology of the particles. For high aspect ratios of the particles forming the preform, wetting angles close to 90°still allow impregnation by the molten metal. The results of the model were confirmed by infiltration of partially sintered TiC preforms with molten Cu and by fabrication of the TiC/Cu composites with various ceramic-to metal ratios. Decreasing the metal content in the composite from 50 vol.% to 10 vol.% leads to a hardness increase from 250 to 1800HV and to the decrease of the bending strength from 960 to 280MPa. The resistivity of these TiC/Cu composites decreases from 142 μohm·cm to 25 μohm·cm.

15th International Plansee Seminar, Eds. G. Kneringer, P. Rödhammer and H. Wildner, Plansee Holding AG, Reutte (2001), Vol. 1

References:

1. V. N. Eremenko, V. V. Fisenko: in "The Role of Surface Phenomena in Metallurgy"(ed. V. N. Eremenko, NY, 1963) pp.117-119
2. P. Xiao and B. Derby: Acta Mater. 44 (1996), pp. 307-314
3. L. Ramqvist : Int. Journal of Powder Metallurgy 1 (1965), pp. 2-8.
4. M. G. Nicholas: in "Surface and Interface of Ceramic Materials" (ed. L. C. Dufour et al., Notwet Kluwer Academic 1989) pp. 375-378
5. A. Gasse, G. Chaumat, C. Rado and N. Eustathopoulos: Journal of Material Science Letters 15 (1996), pp.1630-1633
6. M. G. Nicholas: in "Joining Ceramic, Glass and Metal" (H. Krapits, H. Schaeffer May 17-19 Koningswinter Germany 1993) pp. 15-21
7. V. N. Perevertaylo, A. A. Smekhnov, O. B. Loginova: in Proc. Int. Conf. "High Temperature Capillarity-2", pp. 127-129 (ed. N. Eustathopoulos and N. Sobczak, Foundry Research Institute, Krakow, Poland, 1998)
8. P. Frantz, S.V.Disziulis: Surf. Sci. 412/413 (1998), pp. 384-389
9. R.Souda, T.Aizawa, S. Otani, Y. Ishizawa: Surf. Sci. 256 (1991), pp. 19-24
10. N.Froumin, N.Frage, M. Polak and M.P. Dariel: Acta Mater. 48 (2000), pp. 1435-1441.
11. N. A Travitzky and A. Shlayen: Mater. Sci. Eng. A 244 (1998), pp. 154-159
12. E. J. Gonzalez and K. P. Trumble: J. Amer. Cer. Soc. 79 (1996), pp. 114-121
13. A. Mortensen and T. Wong: Met. Trans. A 21 (1990), pp. 2257-2262
14. A. R. Kennedy, J. D. Wood and B. M. Weager: J. Mat. Sci. 35 (2000) pp.2909-2918
15. K. P. Trumble: Acta Mater. 46 (1998), pp. 2363-2374
16. J. L. Hilden and K. P. Trumble: Material Science Forum (ed. W. A. Kaysser 1999) pp. 308-321.
17. X. F.Yang and X. M Xi,:J. Mat. Sci. 30 (1995), pp. 5099-5104
18. M. Schuhmacher and P. Eveno: Solid State Ionics 12 (1984), pp. 263-266.
19. N. Froumin, N. Frage, M.Polak and M. P. Dariel: Scripta Mater. 37 (1997), pp. 1263-1267